CHAPTER 4
EXPERIMENT: VERIFICATION OF THE ACOUSTIC MODEL AND DETERMINATION OF THE ACOUSTIC LOSS FACTOR

In the preceding chapter, a method to compute the internal acoustic response of a simply-supported cylinder with rigid ends was presented. The solution is based on the Kirchoff-Helmholtz integral and uses the spatial accelerance response of the cylinder wall to compute the internal acoustic response at any point within the cylinder. The radiating structural surface is divided into a set of small discrete surface elements so the K-H integral can be integrated numerically over the entire internal surface of the cylinder. The acoustic boundary element model was also shown to agree with the analytical solution, as presented in Chapter 3. In this chapter the internal acoustic response of the cylinder is measured experimentally. The experimental results are compared to the results predicted by the boundary element model. The comparison is performed for two reasons: the first is to verify the acoustic model and the second is to determine the acoustic loss factor for an acoustic space with very little acoustic damping (similar to a fairing in the low frequency range). The results presented in this chapter validate the acoustic model being used and so both the structural model (Chapter 2) and acoustic model (Chapter 3) can be used to predict the internal acoustic response of a large scale cylinder (which emulates a rocket payload fairing) excited by PZT actuators, as will be presented in Chapter 5.

4.1 Experimental Determination of the Cylinder Structural Operating Shape

In order to test the numerical model used to predict the internal acoustic response of the cylinder, the spatial vibration of the cylinder wall needs to be determined. The SS cylinder described in Chapter 2 is used. In this case the accelerance is measured using a roving accelerometer over a frequency range from 800 to 2400 Hz using a sine-dwell test. A schematic representation of the experiment is shown in Fig. 4.1. The cylinder is excited in phase by PZT actuator "B" (as described in Chapter 2) at 20 Vrms. Two accelerometers are used in the experiment. The first (Kistler 8616A500, SN C49024, 3.79 mV/g) is fixed at a location $x = 270.9$ mm (10.67 in.), $\theta = -17^{\circ}$ throughout all the tests. The purpose of this accelerometer is to verify that the level of actuation is constant from one test to the next. The second accelerometer (Kistler 8620, C46094, 9.88 mV/g) is a roving accelerometer and is used to map the spatial motion of the cylinder. Each accelerometer signal is amplified (Kistler 5122 Piezotron Coupler) 100 times and then channeled to a spectrum analyzer (Tektronix 2630). For each test the roving accelerometer is placed in the appropriate position and the cylinder is excited by actuator B from 800 to 2400 Hz using a sine-dwell measurement. The data is recorded and the test is repeated for a new measurement location. Tests were conducted having the roving accelerometer located at thirteen equally spaced axial locations, $x = 0$, 33.87, 67.73, 101.6,...372.5, 406.4 mm ($x = 0$, 1.33, 2.67, 4,… 14.67, 16 in.) and nineteen equally spaced angular locations ($\theta = 0, 10, 20, \ldots, 180^{\circ}$). Measurements are taken on only half of the cylinder and it is assumed that the results can be mirrored due to the symmetry of the excitation and the mode shapes. A total of 247 distinct measurement locations are mapped on the surface of the cylinder. Once all the individual frequency response functions (FRFs) are obtained, the data is processed and the cylinder spatial operating shape can be determined for a given frequency.

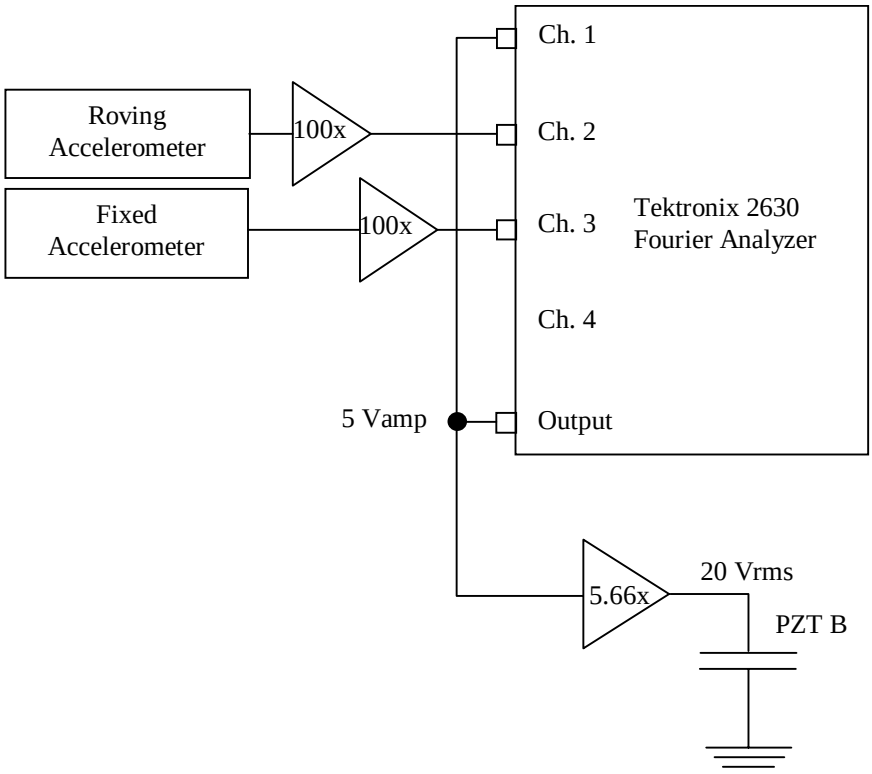

Figure 4.1 Schematic representation of the structural experiment.

4.2 Results of the Cylinder Operating Shape

As described in the section 4.1, the spatial vibration of the cylinder wall needs to be determined in order to verify the numerical model used to predict the internal acoustic response of the cylinder. The purpose of this section is to present the results of the experiment and the respective operating shapes. The FRF of the transverse cylinder displacement at several axial locations ($\theta = 0^{\circ}$) is shown in Fig. 4.2. The location of the resonant frequencies is determined from this figure. Using the data from the experiment described in section 4.1, it is possible to extract the cylinder operating shape at a particular frequency. The magnitude of the operating shape is shown in Fig. 4.3 and Fig. 4.4 at a frequency of 948 Hz. The cylinder operating shape is unwrapped so the results can be more easily graphed and is only shown for half of the cylinder ($\theta = 0^{\circ} - 180^{\circ}$). The spatial displacement pattern clearly indicates that the dominant mode at this frequency is the (2,1) mode. Likewise, the operating shape at 976 Hz can be seen in Fig. 4.5 and 4.6. The displacement pattern indicates that at 976 Hz the operating shape is dominated by the (3,1) structural mode. Operating shapes at other frequencies can be found in Appendix C. The operating shape for the cylinder at a particular frequency is used to calculate the internal acoustic response of the cylinder using the numerical model presented in Chapter 3. The predicted acoustic results, using the measured operating shapes, will be compared to the experimentally measured acoustic results later in this chapter.

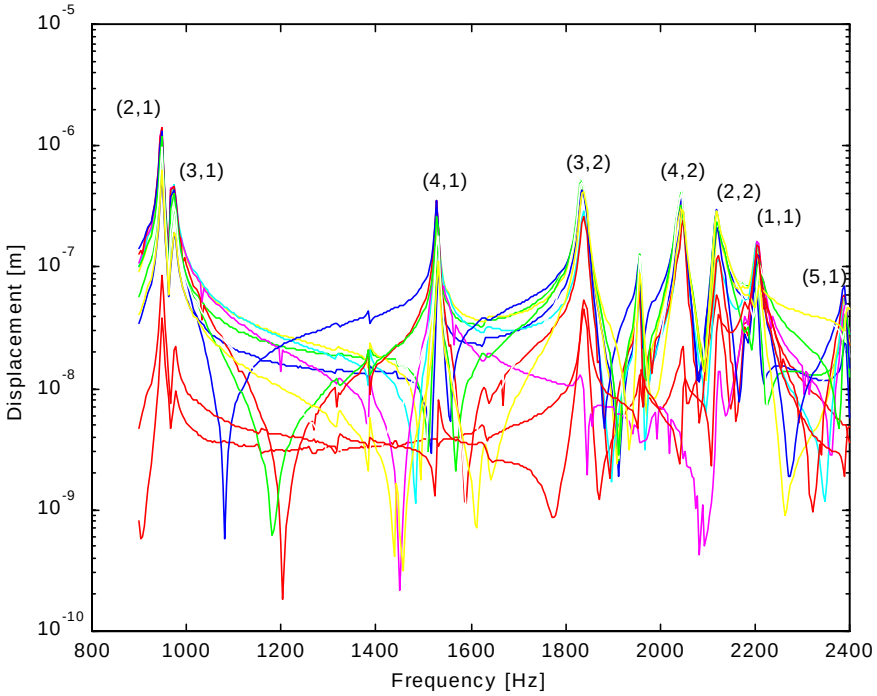

Figure 4.2 Cylinder displacement magnitude at various axial locations, $\theta = 0^{\circ}$.

4.3 Some Experimental Issues and Additional Tests

The experiment described in section 4.2 was conducted over the course of several days due to the large number of measurements taken (247 FRFs). Additional tests were also performed to insure that the experimental results can be considered valid. Since the excitation voltage provided to the PZT actuator was the same in all tests, the signal generated by the fixed accelerometer should not change from one test to the next. Any changes may be due to bonding delamination, actuator cracking, or other unpredictable effects. It was shown that the FRFs produced by the fixed accelerometer for all tests were virtually identical. Also it was thought that the orientation of the accelerometer (right side up or upside down) may affect the acceleration measurement. However it was found that there was no influence in the measurement due to accelerometer orientation. As can be seen in Figs. 4.3 through 4.6, the displacement magnitude at $\theta = 0^{\circ}$ is larger than the displacement magnitude at $\theta = 180^{\circ}$ (test performed one week later). This is an unexpected result since the mode shape of the cylinder is symmetric. It is believed that the difference in displacement magnitude is attributed to subtle changes in the resonant frequency of the cylinder due to temperature and time effects. Since the resolution of the sine-dwell test is 4 Hz, it is likely that the exact location of the resonant frequency is between measurements. Small changes in the resonant frequencies will cause the magnitude of the measured operating shape to change from one measurement to the next. Also, it was shown that the maximum vibration of the endplate was between one and two orders of magnitude less than the maximum vibration of the cylinder wall. It is believed that these small changes in the operating shape measurement and the endplate vibration have a minimal effect on the computation of the internal acoustic response of the cylinder. Lastly, it should be reiterated that a structure's modal natural frequency and the resonant frequency are not the same. In the work presented in Chapter 2, the cylinder's resonant

frequency is used to approximate the location of the modal natural frequency. Limitations of this assumption are discussed in Appendix I. As is seen in Fig. 4.3 and 4.5, adjacent mode coupling exists at these resonant frequencies.

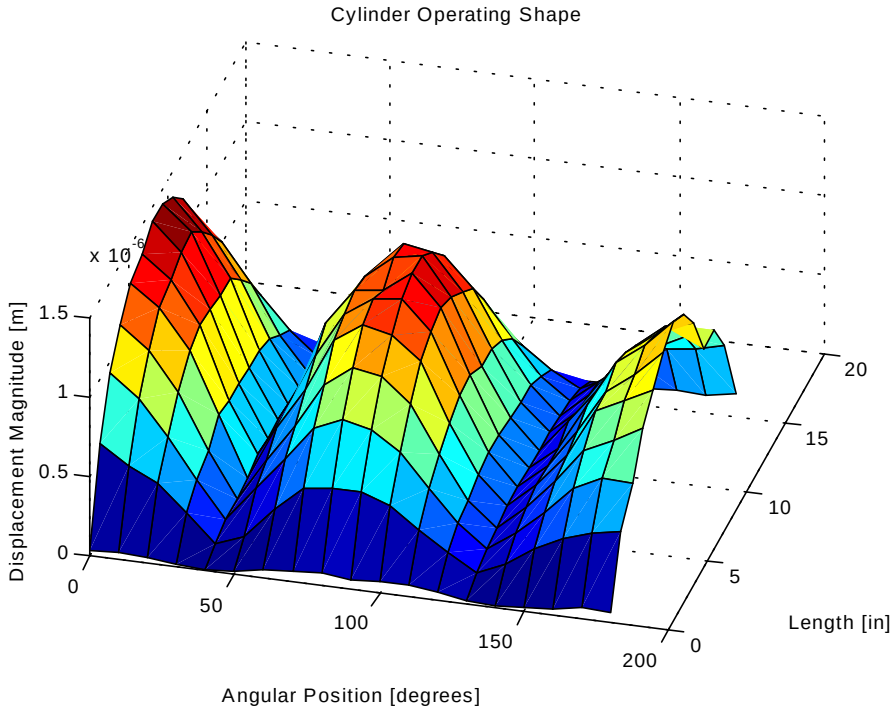

Figure 4.3 Cylinder operating shape at 948 Hz (2,1).

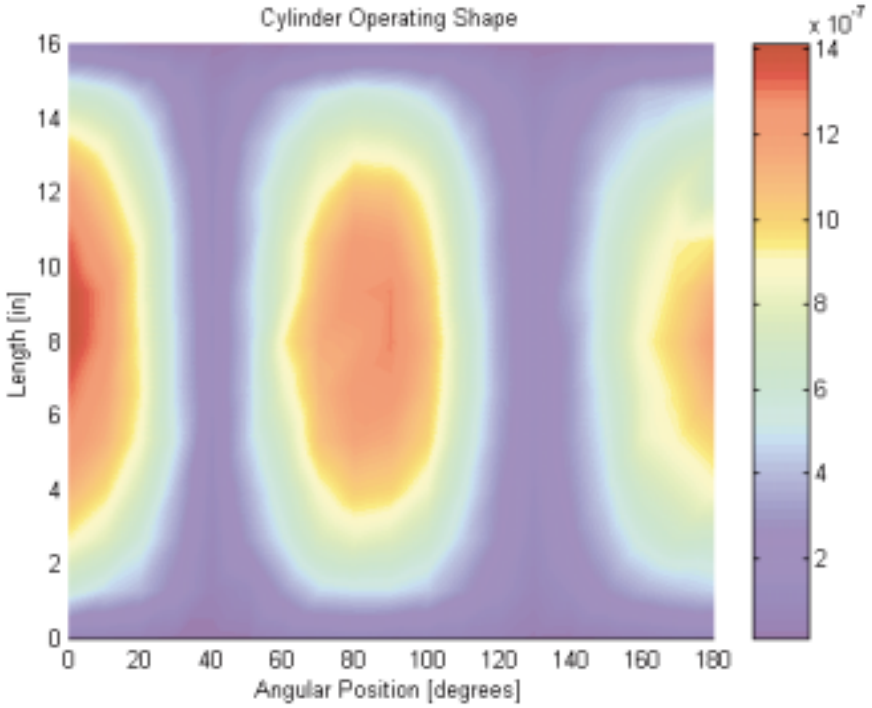

Figure 4.4 Cylinder operating shape at 948 Hz, (displacement magnitude, m).

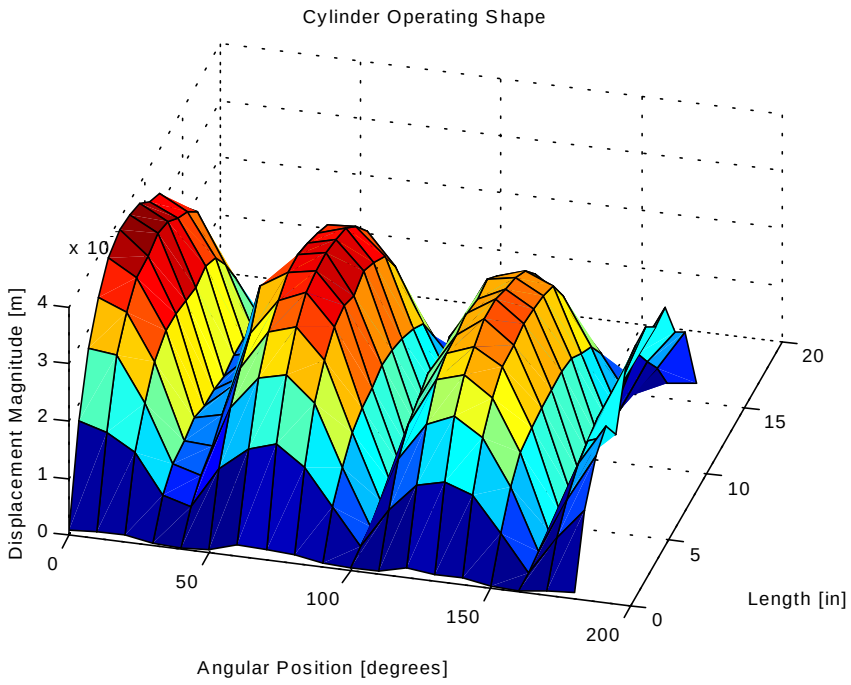

Figure 4.5 Cylinder operating shape at 976 Hz (3,1).

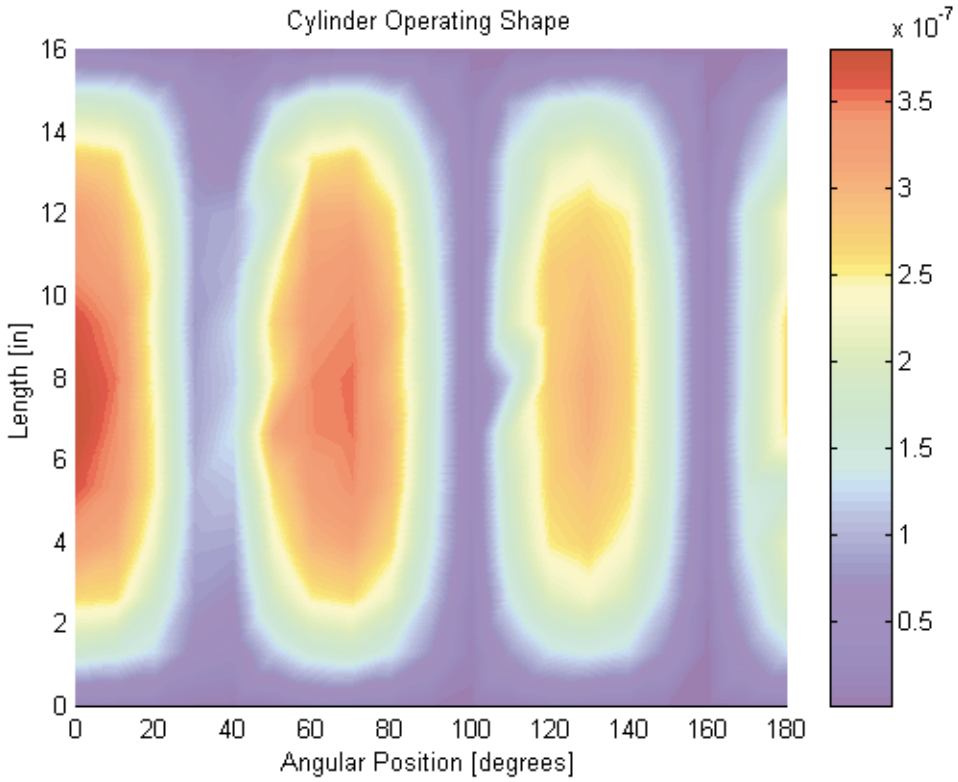

Figure 4.6 Cylinder operating shape at 976 Hz, (displacement magnitude, m).

4.4 Description of the Acoustic Experimental Setup

In order to measure the acoustic response within a simply-supported (SS) cylinder, the cylinder described in chapter 2 is used. The physical orientation of the microphones used to measure the internal acoustic response within the cylinder during the experiment is shown in Fig. 4.7. The test apparatus consists of three Radio Shack Optimus (RSO) microphones attached to a sliding microphone boom. The boom is made from a ¼ inch Al tube which houses the six wires for the three microphone signals (A, B, and C). The boom is designed such that the axial and angular position of the microphones within the cylinder can be changed. The radial position of the three microphones is fixed and is described in Table 4.1. The microphones were calibrated with respect to a B&K Type 4191 (SN 2017323) microphone. The details of the calibration process can be found in Appendix D. To obtain absolute values of acoustic pressure within the cylinder, the microphones are configured as shown in Fig. 4.8.

The three microphone signals are conducted using the wires within the boom. The corresponding signals are then conditioned using the pre-amplifiers supplied with these RSO microphones. The signals are then amplified 50 times using several Frequency Devices LPO1 filters, operating in by-pass mode and sent to the corresponding channel of the analyzer. The 5V (amplitude) output from the analyzer is entered to channel 1 as a reference signal to obtain absolute acoustic levels from the experiment. The reference signal is also amplified approximately 5.66 times by a 790 Series AVC Power Amplifier, so the PZT voltage is approximately 20 Vrms. The same cylinder excitation is used in these tests as the in the tests performed in section 4.3.

Table 4.1 Radio Shack Optimus microphone properties

Microphone	A	B	C
Type	33-3013	33-3003	33-3003
Radial Position (in.)	0.85	2.6	4.35
Sensitivity (mV/Pa)	4.23	4.96	4.91

4.5 Description of the Acoustic Measurements

In order to determine the acoustic modal properties of the cylinder, the measurements within the cylinder are taken using the three RSO microphones (A, B, and C) attached to the acoustic boom. Since the radial orientation of the microphones is fixed, slices of the acoustic field can be obtained by either rotating the boom while keeping the axial position fixed or by sliding the boom in the axial direction while keeping the angular position fixed. In this experiment the acoustic field within the cylinder is mapped from 800 to 2400 Hz while using an excitation equivalent to that described in section 4.1. The cylinder is excited in phase by PZT actuator “B” at 20 Vrms. The acoustic field is mapped in a vertical slice at the center of the cylinder along its length. Starting with the microphones located 19.05 mm (0.75 in.) away from the endplate

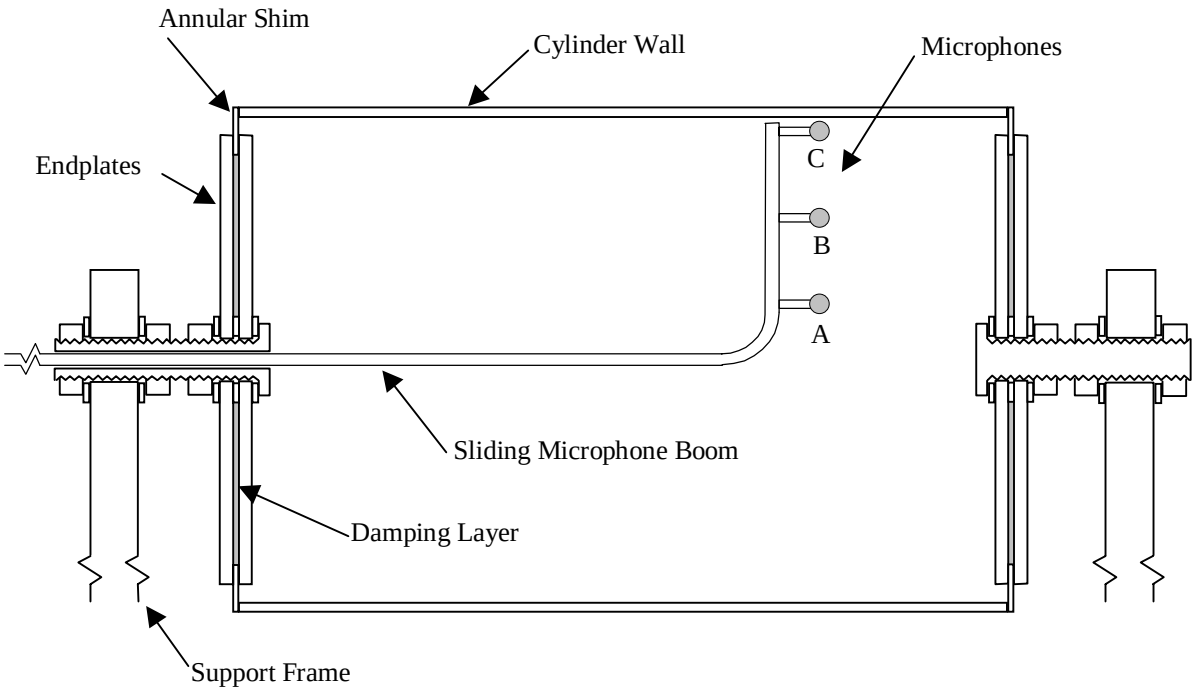

Figure 4.7 Cross section of the acoustic test set up.

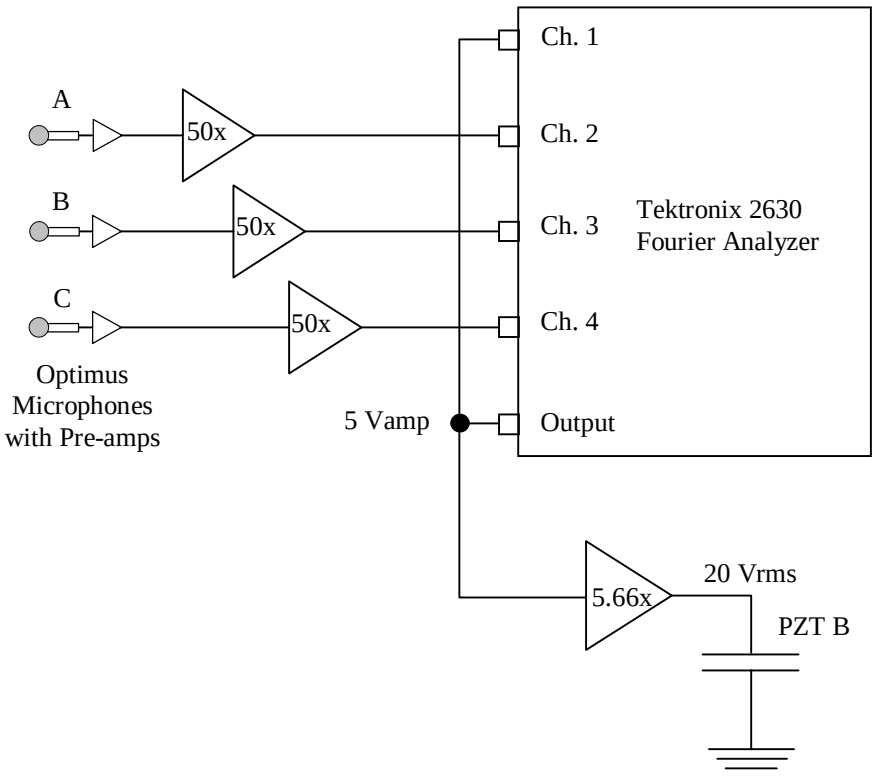

Figure 4.8 Schematic of the microphone and actuator signal conditioning.

interior surface ($\theta = 0^{\circ}$), measurements are taken using a sine-dwell test from 800 to 2400 Hz. The acoustic boom is then shifted 12.7 mm (0.5 in.) in the axial direction and the measurement is repeated. The process is continued until the last measurement located at 323.85 mm (12.75 in.) from the endplate interior surface. The boom then rotated 180 degrees and the process is repeated. The measurements can then be processed to create an axial acoustic field as shown in Fig. 4.9. The purpose of mapping the axial field (vertical plane of measurements) is to determine the corresponding axial acoustic modal index (i). Likewise to obtain the angular modal index (j) the acoustic field needs to be mapped in the angular direction. To do this, the microphones are placed in a desired axial position and then the acoustic boom is rotated from 0 to 180 degrees. In this experiment three different axial positions are chosen to map the acoustic field in the angular direction. The first is located 19.05 mm (0.75 in.) from the endplate interior surface ($\theta = 0^{\circ}$). Measurements are taken from 800 to 2400 Hz and then the boom is rotated 10 degrees and the measurement is repeated. The process is continued until the last measurement is taken at 180 degrees. It is assumed that the acoustic field is symmetric and can be mirrored about the vertical axis. Two additional acoustic slices are taken at 130.56 mm (5.14 in.) and 195.83 mm (7.71 in.) from the surface of the endplate. These positions represent 1/3 and 1/2 the acoustic length of the cylinder, respectively. The radial slices are shown in Fig. 4.10. It should be noted that in this experiment the radial modal index (k), which varies as a Bessel function in the radial direction, is not definitively determinable due to the lack of measurements in the radial direction.

It should also be mentioned that the acoustic measurements were taken over the course of several days. To insure the validity of the tests, several acoustic measurements performed at the beginning of the testing period were repeated at the end. The results from both tests were virtually identical. Also the fixed accelerometer (described in section 4.1) used to measure the structural response of the cylinder was also used to verify that the vibration of the cylinder had not changed during testing. The vibration measurement of the cylinder at the beginning and end of the testing period produced identical results to those described in section 4.1.

4.6 Results of the Acoustic Natural Frequencies for the Cylinder

The acoustic response of the cylinder to the excitation caused by PZT actuator B at (20 Vrms) is shown in Fig. 4.11. In the figure, the various lines represent the response measured by microphones A, B, and C at three different boom locations. All the measurements are taken in the vertical plane ($\theta = 0^{\circ}$) at the three different axial locations where the radial slices are mapped (described in section 4.5). These points are chosen since the actuator aligns the acoustic mode shapes in the vertical plane and so the maximum acoustic response is expected at these points. The peaks in the response are dominated by either structural modes (S) or acoustic modes (A). Peaks believed to be dominated by an acoustic mode with a Bessel component are also indicated (B). The procedure to identify the acoustic mode corresponding to a resonance (peak) is presented in the next section. The analytical and experimental natural frequencies are compared in Table 4.2 and Figs. 4.12 and 4.13. For those modes which are detectable experimentally, the maximum absolute difference between the analytical natural frequencies (for a closed circular cylinder) and the measured natural frequencies is at most 14.3 Hz, occurring at the (5,1,0) mode. The average difference is only 4.6 Hz for the sixteen detected modes.

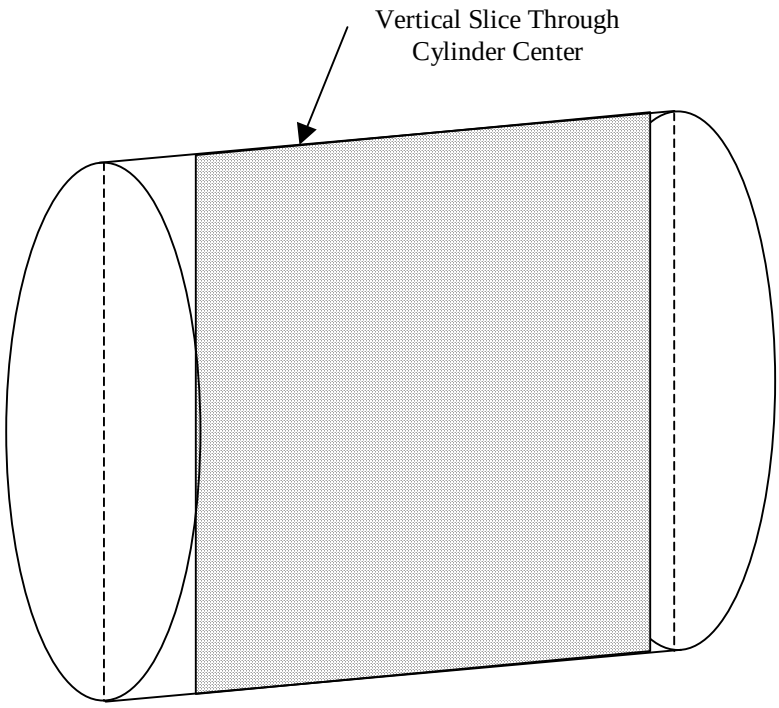

Figure 4.9 Vertical plane of acoustic field measurements.

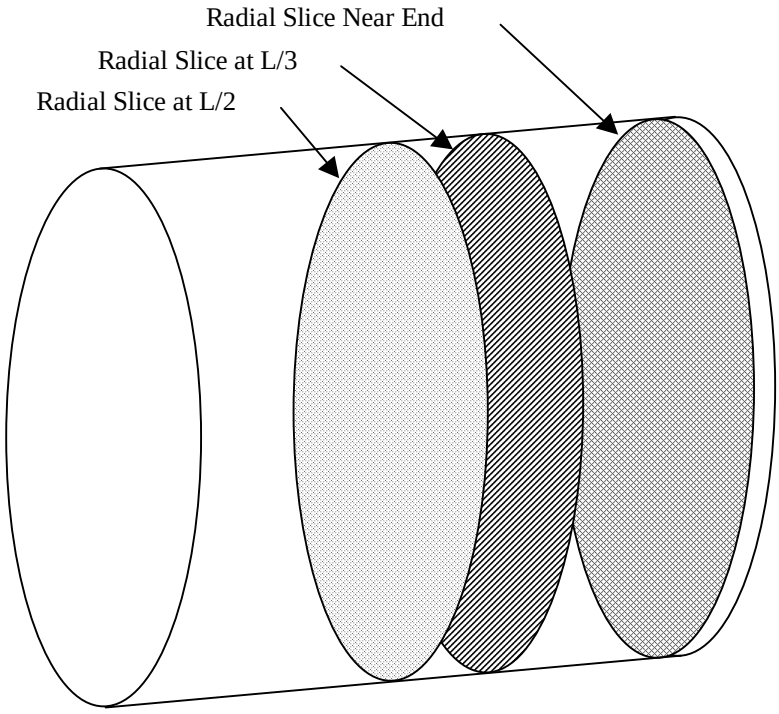

Figure 4.10 Radial planes of acoustic field measurements.

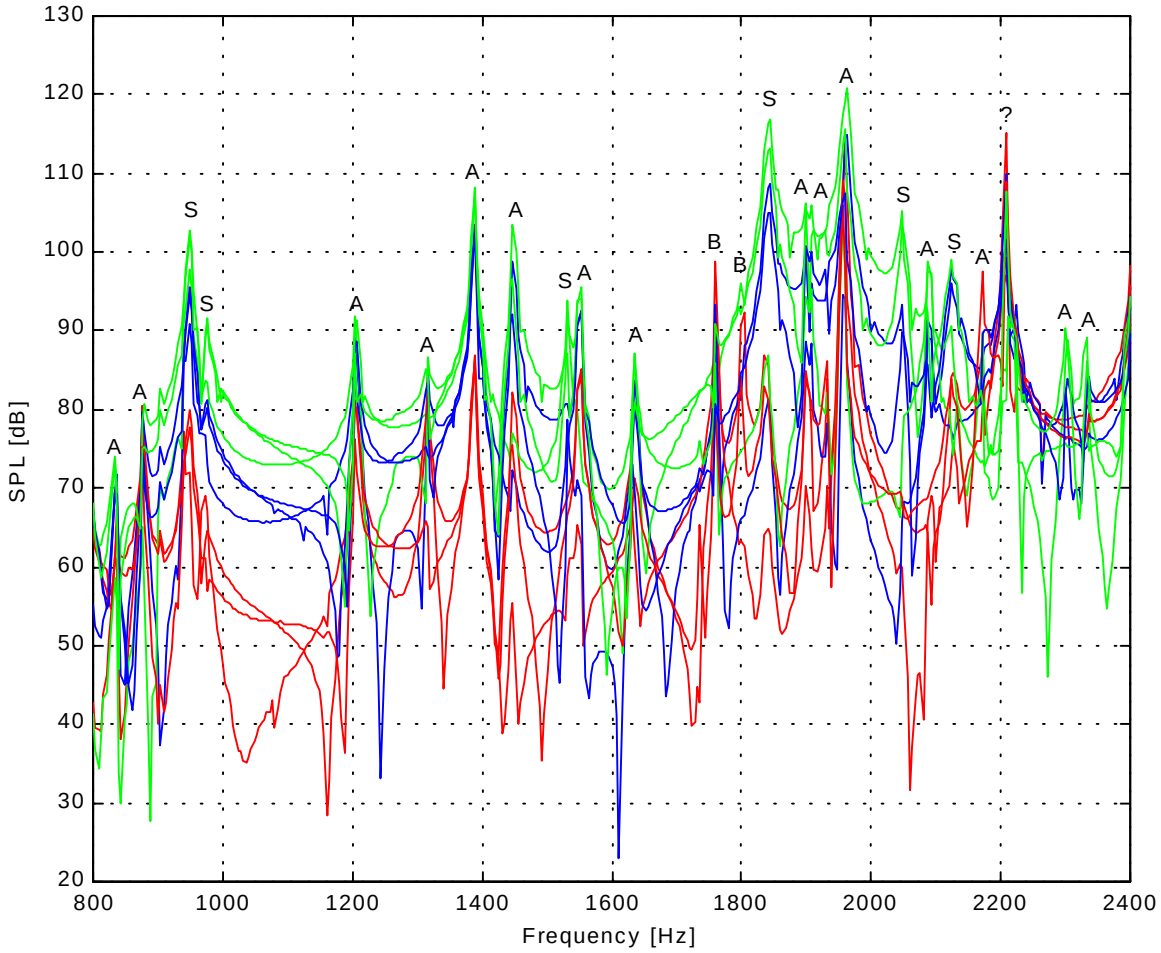

Figure 4.11 Acoustic response of the cylinder at $\theta = 0^{\circ}$ for microphones A, B, & C; near the endplate, at L/2, and L/3 (S=structural mode, A=acoustic mode, B=Bessel mode, ?=unknown).

Some of the analytical modes are not detected in this experiment but can be explained. The (1,1,0) mode should occur at 941 Hz but is buried by the influence of the (2,1) structural mode occurring at 948 Hz, which excites the (0,2,0) acoustic mode of the cylinder. The (0,0,1) and (1,0,1) acoustic modes are difficult to measure because of the number of measurement points required to view the Bessel function influence in the radial direction. The (4,0,0), (4,1,0), and the (2,0,1) are not well excited because they do not couple well with the nearby structural modes {(3,2), 1838 Hz; (4,2), 2044 Hz}. The (5,0,0) and (4,2,0) modes are not excited by the structure and are also difficult to measure due to the measurement resolution in the axial direction.

It is interesting to note that as expected the acoustic and structural modes for a cylinder couple only if they have matching circumferential modal indices. Likewise, the axial modal indices have to be an even/odd combination for coupling to occur.

Table 4.2 Comparison of analytical and experimental natural frequencies

	Modal index (i, j, k)	Analytical f_n (Hz)	Experimental f_n (Hz)	Error (Hz)
1	1,0,0	437.8	439.5	1.7
2	0,1,0	833.1	832	-1.1
3	2,0,0	875.7	876	0.3
4	1,1,0	941.1	-	-
5	2,1,0	1208.6	1208	-0.6
6	3,0,0	1313.5	1316	2.5
7	0,2,0	1381.9	1388	6.1
8	1,2,0	1449.6	1452	2.4
9	3,1,0	1555.4	1552	-3.4
10	2,2,0	1636	1636	0
11	0,0,1	1733.7	-	-
12	4,0,0	1751.3	-	-
13	1,0,1	1788.1	-	-
14	0,3,0	1900.9	1908	7.1
15	3,2,0	1906.6	1900	-6.6
16	4,1,0	1939.4	-	-
17	2,0,1	1942.3	-	-
18	1,3,0	1950.7	1964	13.3
19	2,3,0	2092.9	2088	-4.9
20	3,0,1	2175.1	2172	-3.1
21	5,0,0	2189.2	-	-
22	4,2,0	2230.9	-	-
23	3,3,0	2310.6	2304	-6.6
24	5,1,0	2342.3	2328	-14.3

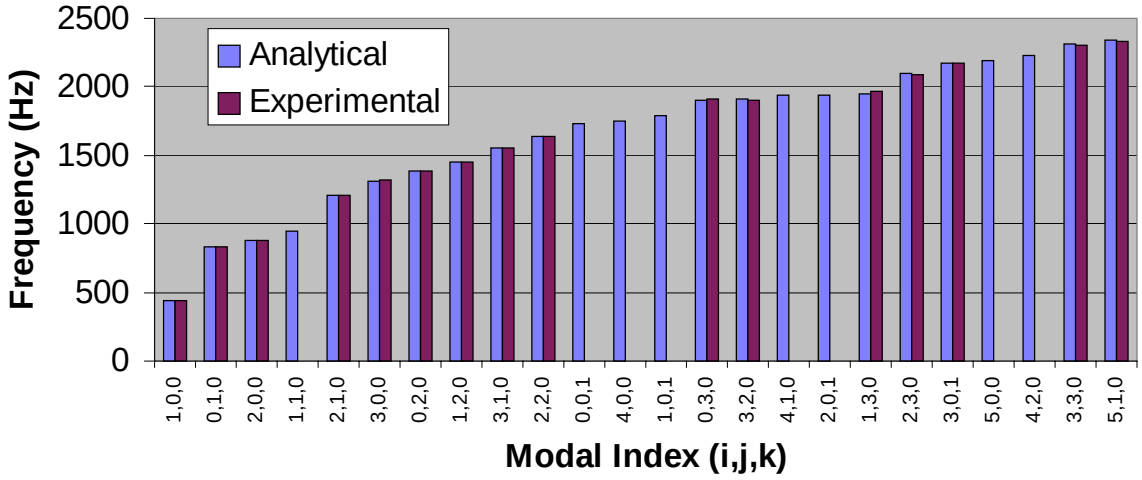

Figure 4.12 Comparison of analytical and experimental acoustic natural frequencies.

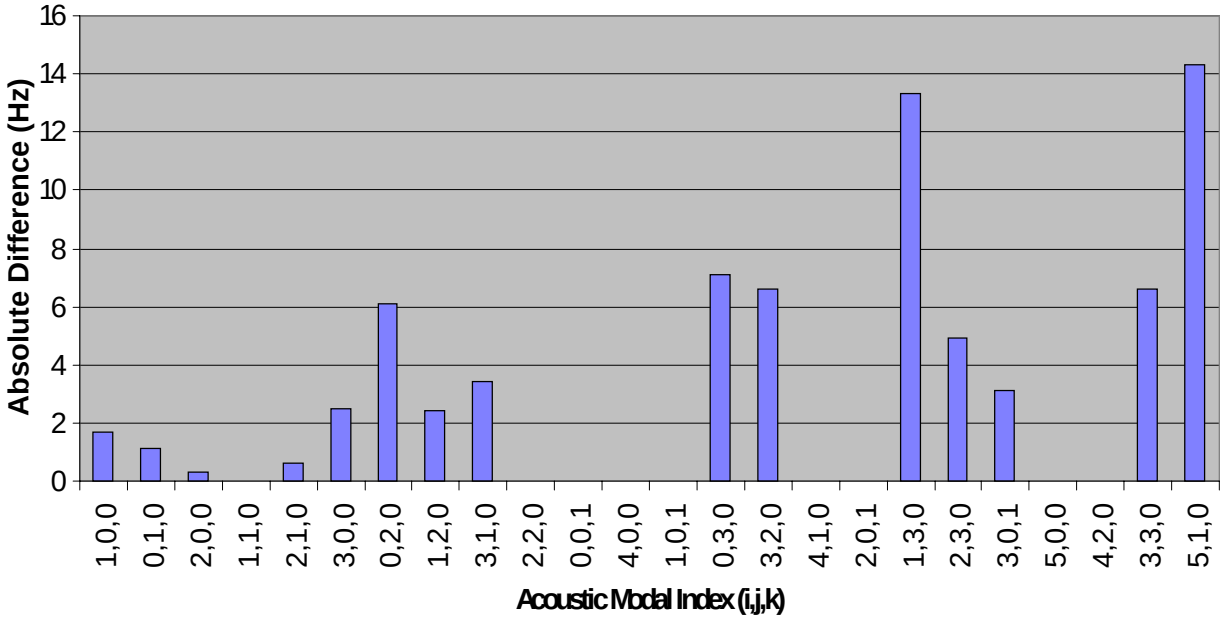

Figure 4.13 Error between the analytical and experimental acoustic natural frequencies.

4.7 Determination of the Acoustic Modes

As described in section 4.5, the axial and radial acoustic fields within the cylinder need to be viewed in order to determine which acoustic mode corresponds with the associated peaks (resonances) presented in Fig. 4.11. Presented in Figs. 4.14 – 4.17 are the axial and radial acoustic field slices at 948 Hz. The axial field is uniform, there exists two nodal diameters, and there are no nodal circles (Bessel contribution). By perusing the graphs it can be concluded that the acoustic field within the cylinder is similar in shape to the (0,2,0) acoustic mode. Even though there is no acoustic mode at this frequency, 948 Hz coincides with the (2,1) structural mode of the cylinder. It is expected that the (2,1) structural mode couples best with the (0,2,0) acoustic mode located at 1388 Hz. It can therefore be concluded that the acoustic peak at 948 Hz is caused by the (2,1) structural resonance. As another example, presented in Figs. 4.18 – 4.21 are the axial and radial acoustic field slices at 1552 Hz. The axial field in this case has three distinct nodal lines, one nodal diameter, and no nodal circles. This pattern is clearly indicative of the (3,1,0) acoustic mode. Due to space limitations, the remainder of the acoustic field slices can be found in Appendix E.

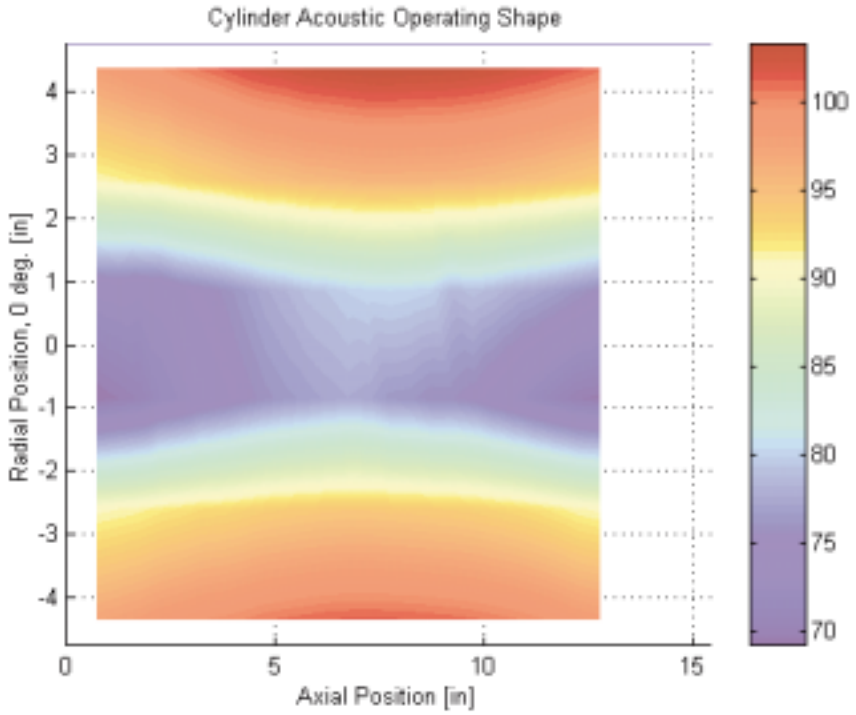

Figure 4.14 Axial internal acoustic field (SPL in dB) at 948 Hz.

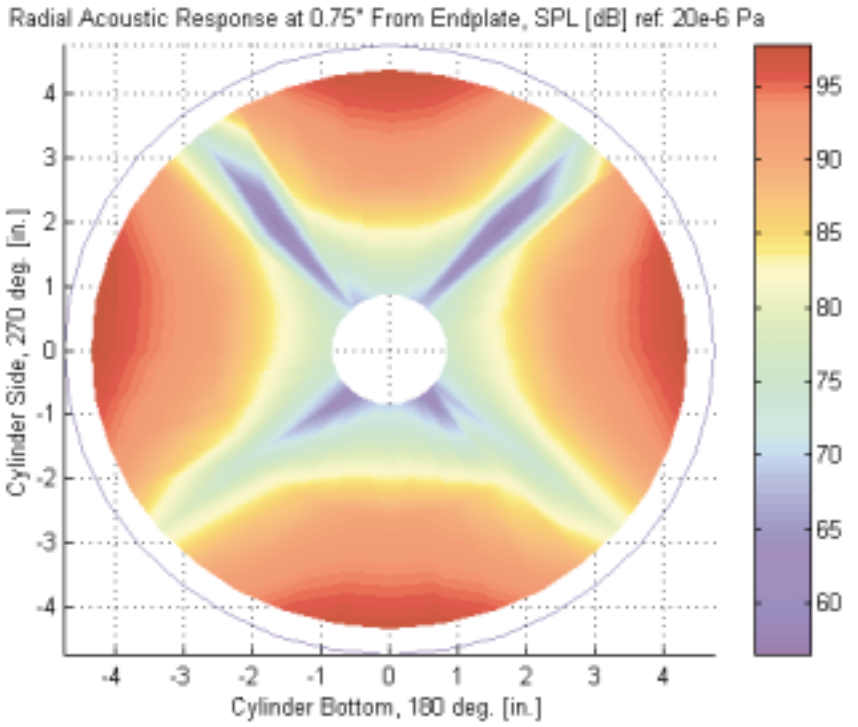

Figure 4.15 Radial internal acoustic field near endplate (SPL in dB) at 948 Hz.

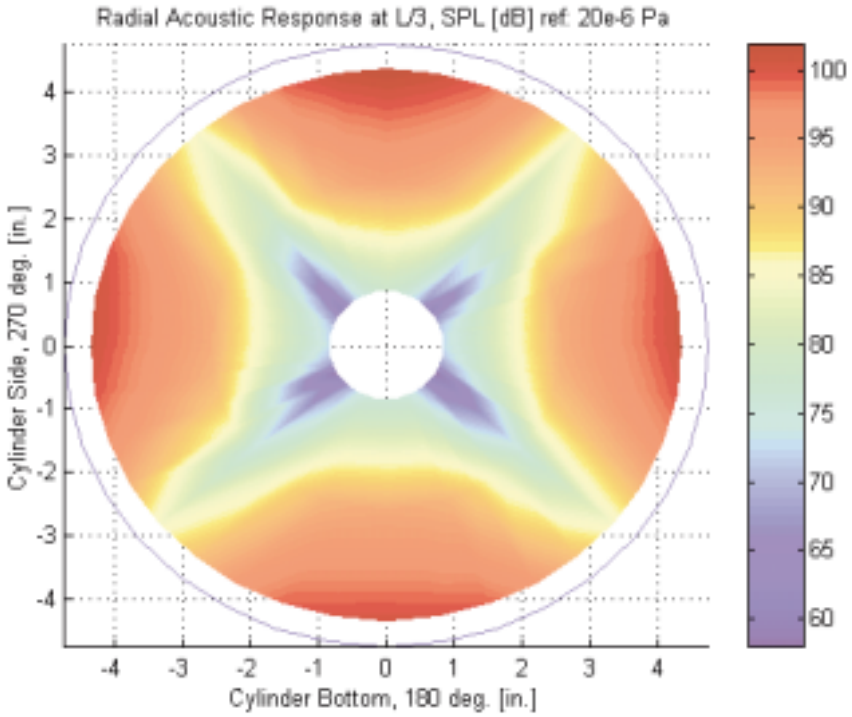

Figure 4.16 Radial internal acoustic field at 1/3 cylinder length, (SPL in dB) at 948 Hz.

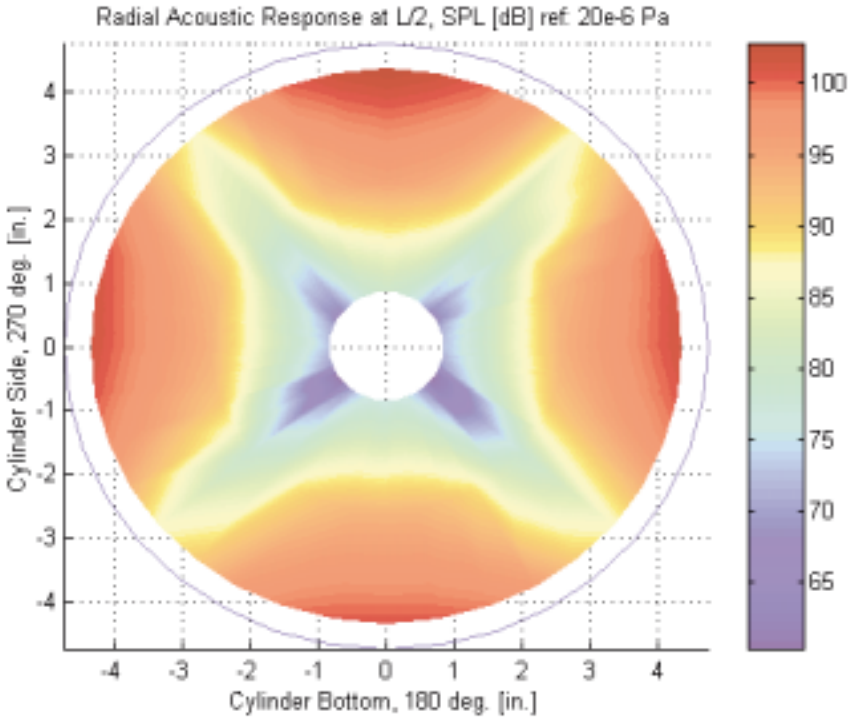

Figure 4.17 Radial internal acoustic field at 1/2 cylinder length, (SPL in dB) at 948 Hz.

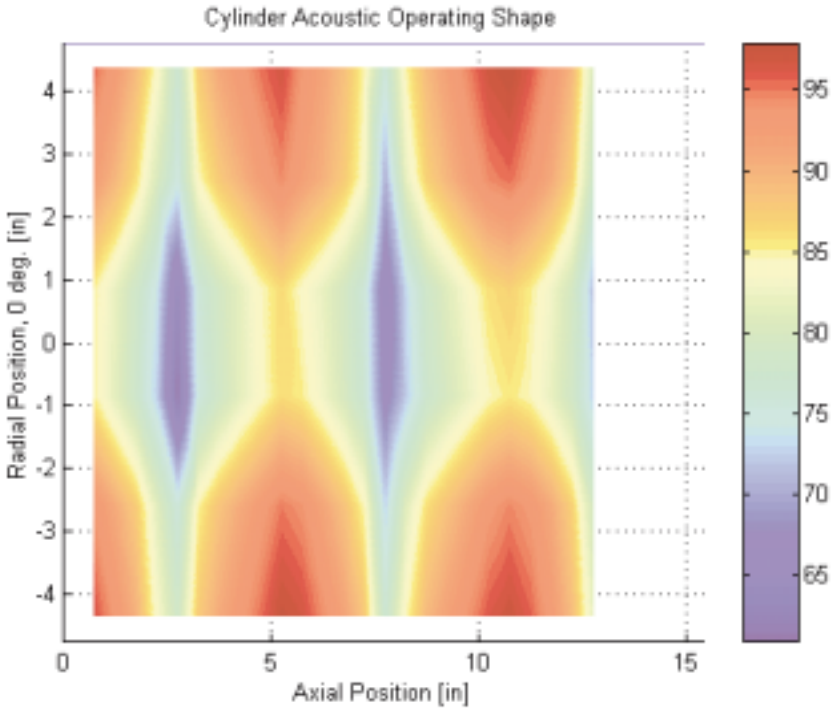

Figure 4.18 Axial internal acoustic field (SPL in dB) at 1552 Hz.

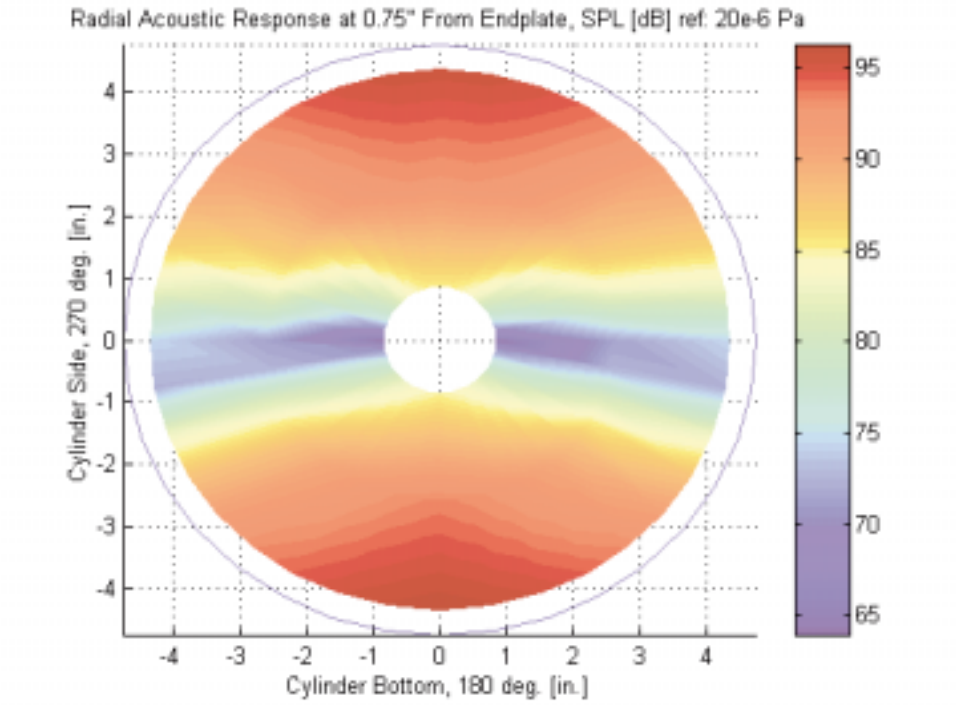

Figure 4.19 Radial internal acoustic field near endplate (SPL in dB) at 1552 Hz.

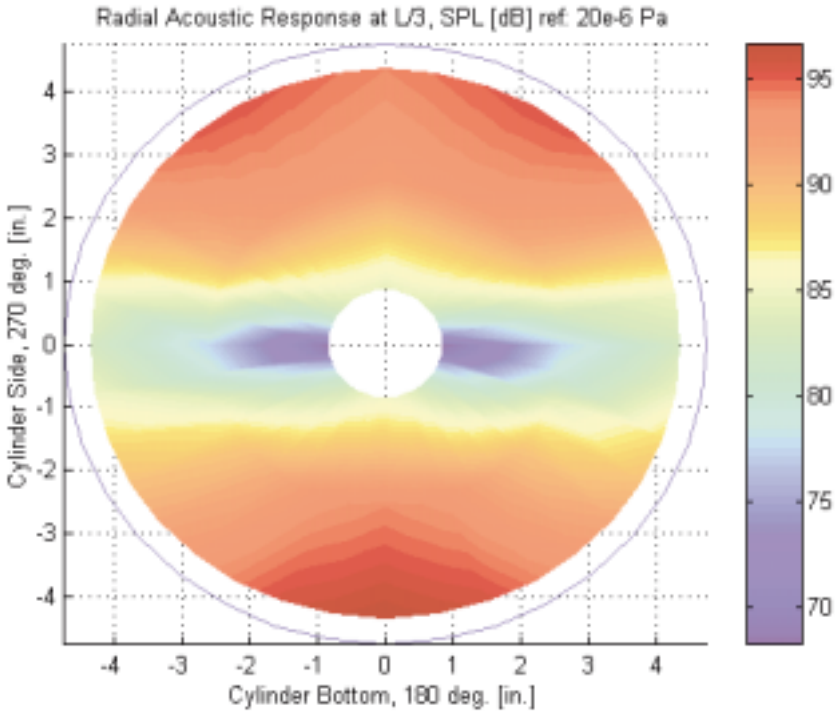

Figure 4.20 Radial internal acoustic field at 1/3 cylinder length, (SPL in dB) at 1552 Hz.

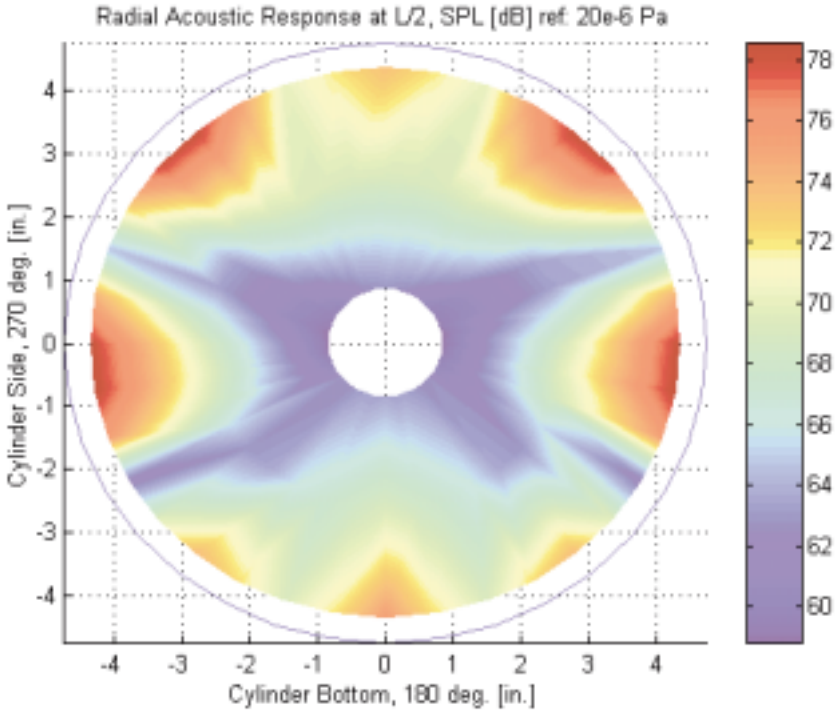

Figure 4.21 Radial internal acoustic field at 1/2 cylinder length, (SPL in dB) at 1552 Hz.

4.8 Effect of Changes to the Acoustic Loss Factor

Inclusion of an acoustic loss factor is one way to include damping into the analytical and numerical solution for the internal acoustic response of the cylinder. The loss factor influences the value of the Green's function by affecting the denominator of Eq. 3.4. The wavenumber is given by,

$$\kappa = \frac{\omega}{c} \tag{4.1}$$

where, ω and c represent the angular frequency and complex wave speed, respectively. The loss factor is introduced by affecting the wave speed where,

$$c = c_o(1 + \imath\eta_a) \tag{4.2}$$

where, c_o, $\imath$, and η_a represent the acoustic wave speed in air (343 m/s), an imaginary number, and the acoustic loss factor, respectively. By introducing a small complex component to the speed of sound, damping is introduced to the solution of the acoustic response.

Other authors have also included damping into their models in a similar way, however comparisons between the assumed and actual values are somewhat limited (Silcox and Lester, 1989, Bullmore et al., 1987, Bullmore et al., 1986).

Shown in Fig. 4.22 is the predicted acoustic response within the cylinder { x_{ac} = 19.05 mm (0.75 in.), r = 110.49 mm, (4.35 in.), $\theta = 0^\circ$, location similar to microphone C} for three different values of acoustic loss factor (1, 0.5, and 0.1 %). The variable x_{ac} refers to the distance from the inside surface of the endplate in the axial direction. As expected, the lowest loss factor produces the curve with the highest peaks. Also, the changes in the loss factor have little effect on the magnitude of the acoustic response away from the acoustic resonance. This is also found to be true at the peaks controlled by the cylinder structural resonances (indicated with an "S" in Fig. 4.22). The loss factor influences the magnitude of the acoustic response near the acoustic resonances.

4.9 Comparison of the Model with Experiment

A comparison between the predicted numerical model and the experimental results is presented in this section. For all of the results presented herein, a loss factor of 0.1% is used. This value produces a close match between the magnitude of the numerical and experimental acoustic response. The acoustic SPLs predicted by the model are compared to the experimental results in Figs. 4.23-4.25 for three different axial positions { r = 110.49 mm, (4.35 in.), $\theta = 0^\circ$, location similar to microphone C}. The corresponding phase information can be found in Appendix H. Clearly the model is able to predict the acoustic behavior within the cylinder at all three axial positions. Most of the resonances and anti-resonances are predicted with only slight shifts in frequency. The simulated spatial acoustic pattern at 948 Hz is also shown in Figs. 4.26-4.29. The predicted acoustic field is similar to the result produced experimentally as previously shown in Figs. 4.14-4.17. The simulated spatial acoustic pattern at 1552 Hz is also shown in Figs. 4.30-4.33. The simulated results are comparable to the experimentally determined results previously

shown in Figs. 4.18-4.21. Both the simulated and experimentally measured fields are very similar.

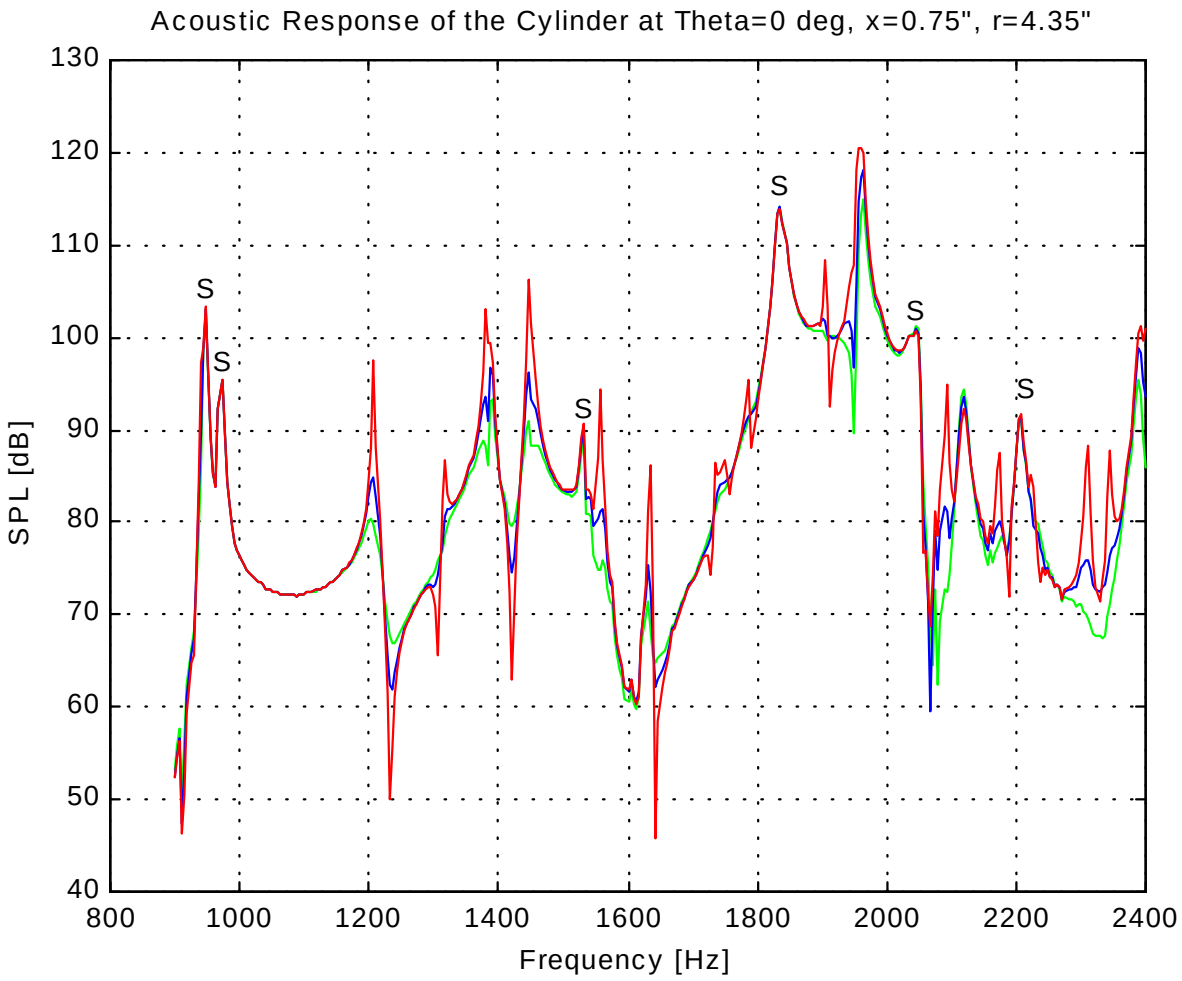

Figure 4.22 Model acoustic response for various acoustic loss factors (1, 0.5 and 0.1%).

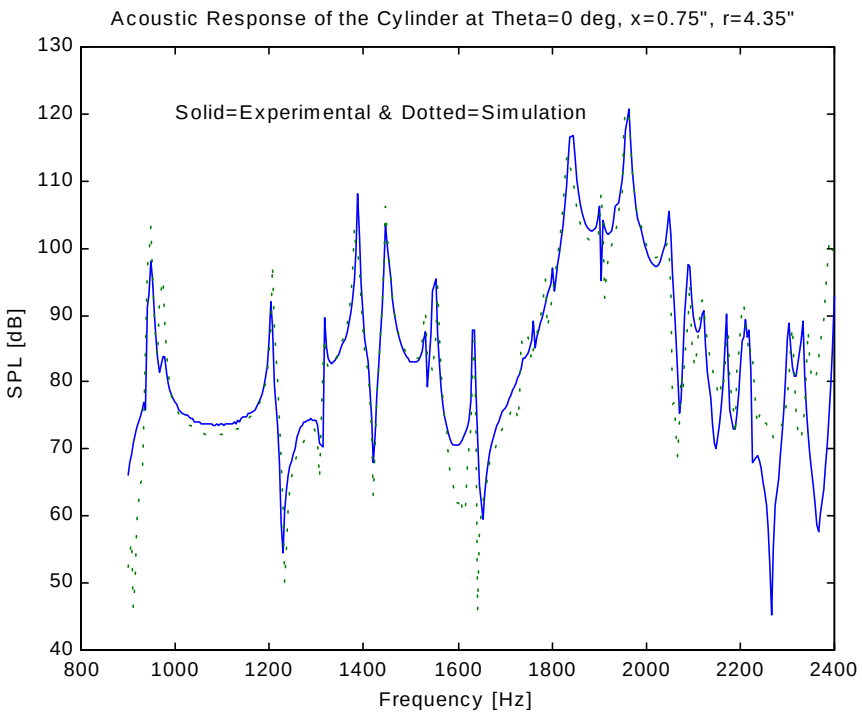

Figure 4.23 Comparison of the acoustic simulation with experiment { x_a = 19.05 mm (0.75 in.)}.

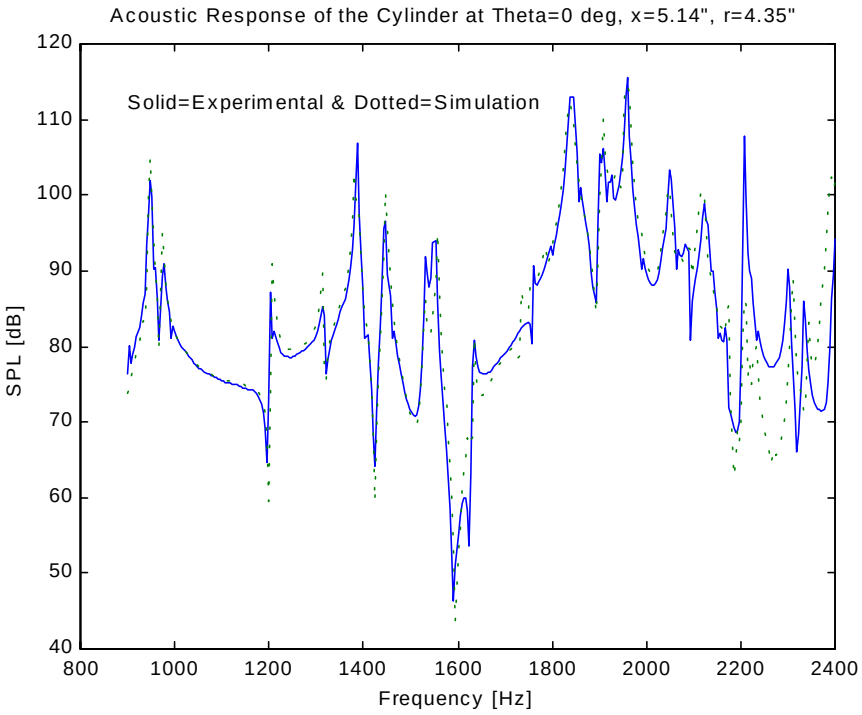

Figure 4.24 Comparison of the acoustic simulation with experiment { x_a = 130.56 mm (5.14 in.)}.

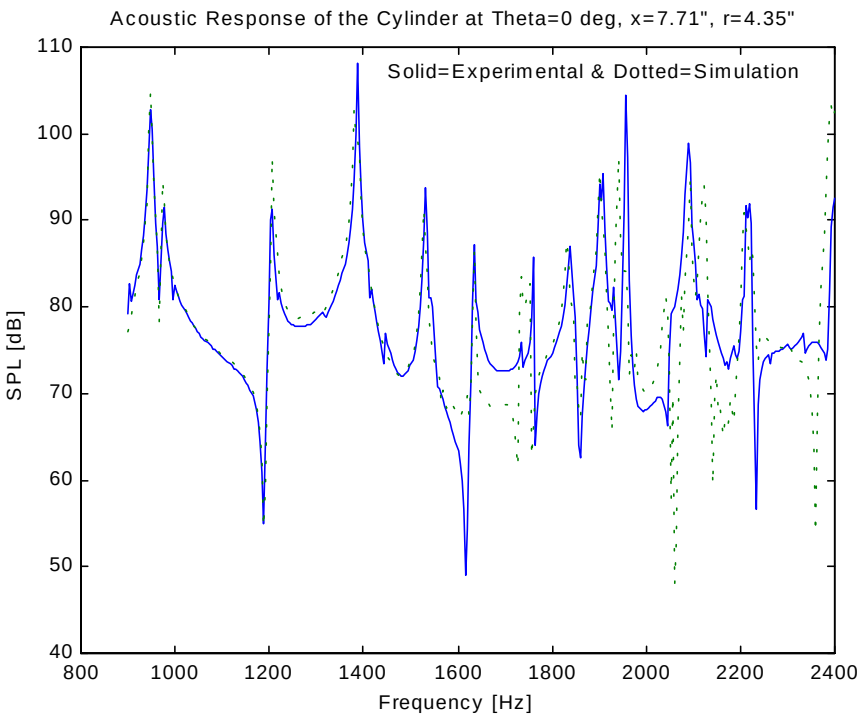

Figure 4.25 Comparison of the acoustic simulation with experiment { x_a = 195.83 mm (7.71 in.)}.

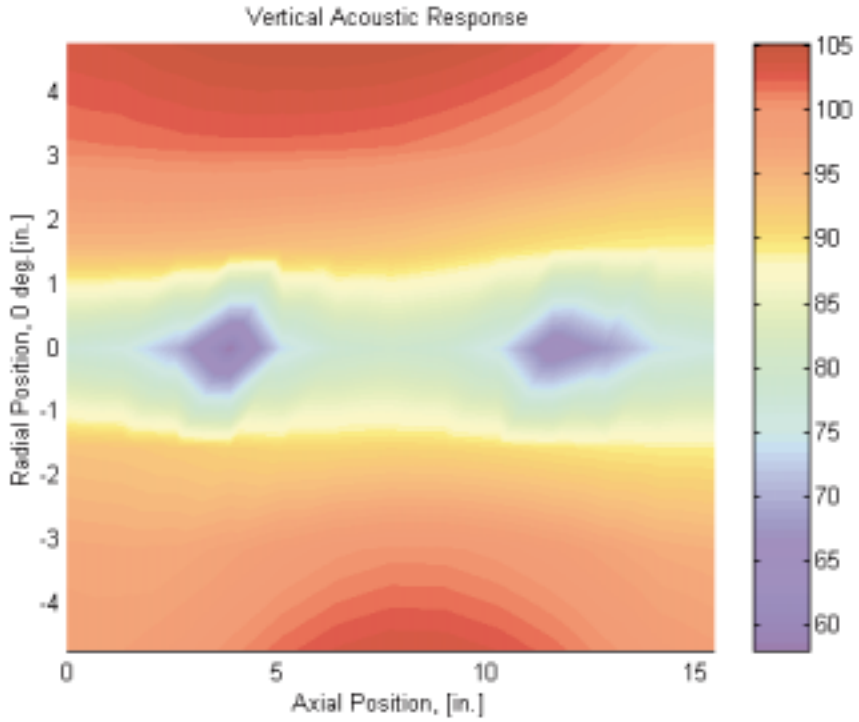

Figure 4.26 Axial internal acoustic simulation (SPL in dB) at 948 Hz.

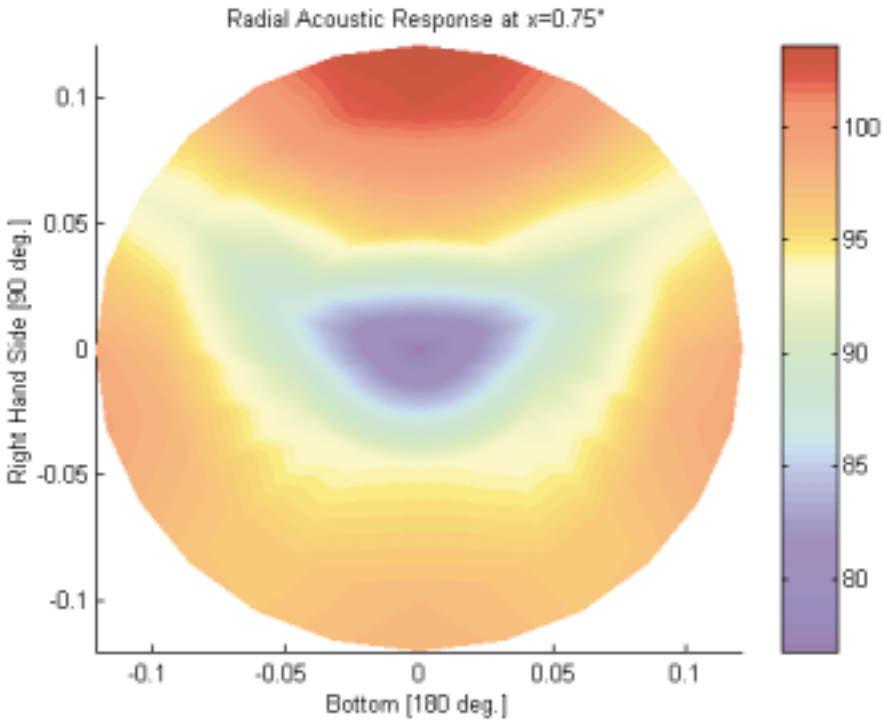

Figure 4.27 Radial internal acoustic simulation near endplate (SPL in dB) at 948 Hz.

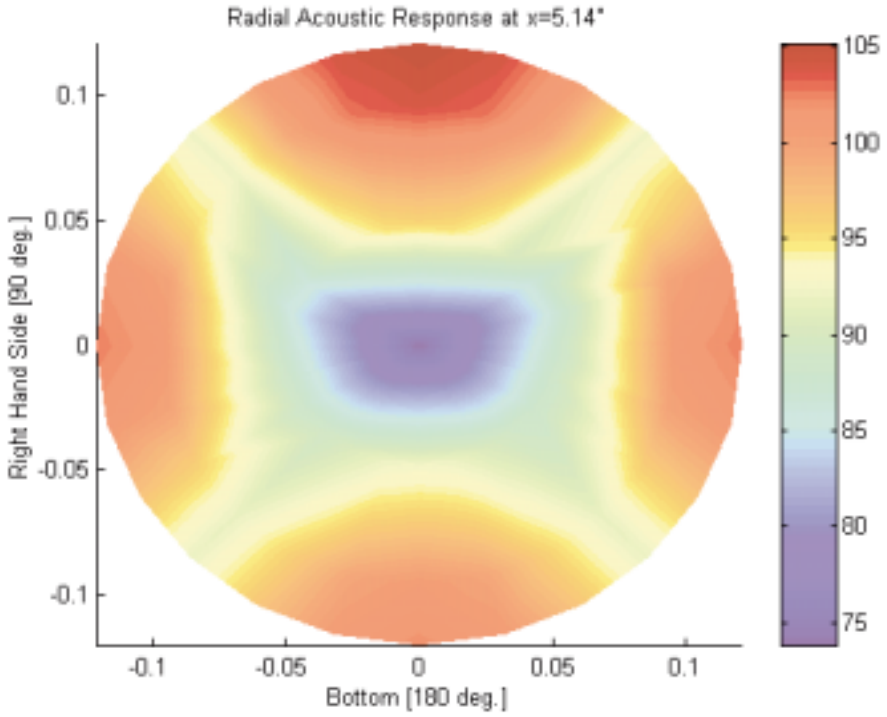

Figure 4.28 Radial internal acoustic simulation at 1/3 cylinder length (SPL in dB) at 948 Hz.

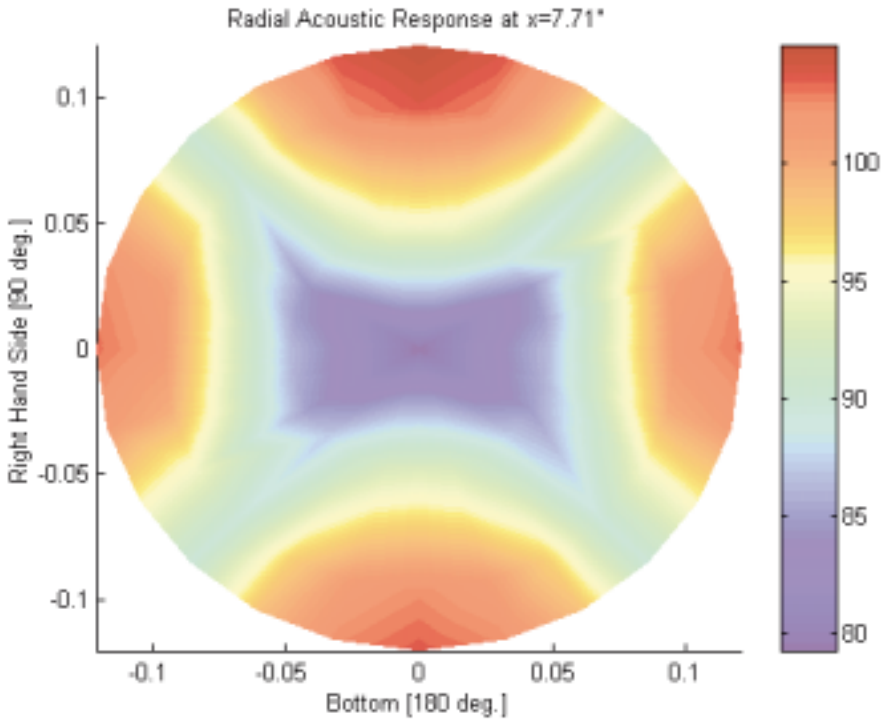

Figure 4.29 Radial internal acoustic simulation at 1/2 cylinder length (SPL in dB) at 948 Hz.

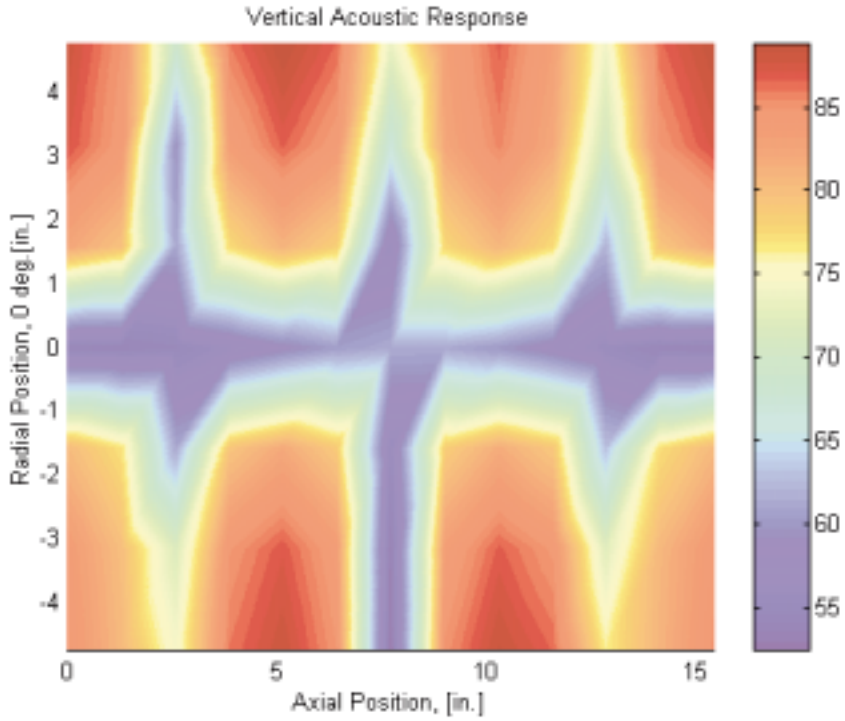

Figure 4.30 Axial internal acoustic simulation (SPL in dB) at 1552 Hz.

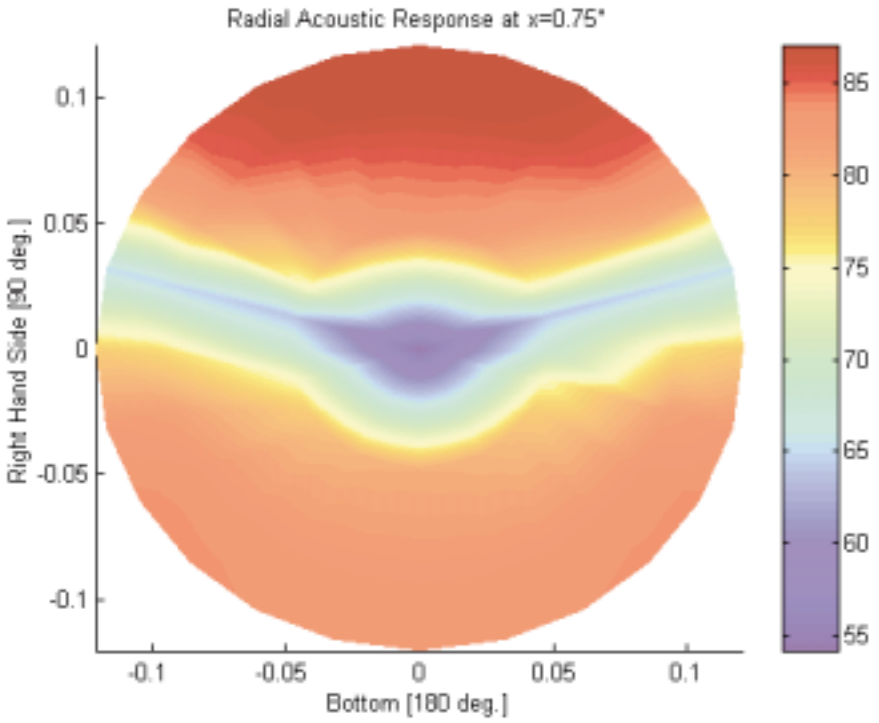

Figure 4.31 Radial internal acoustic simulation near endplate (SPL in dB) at 1552 Hz.

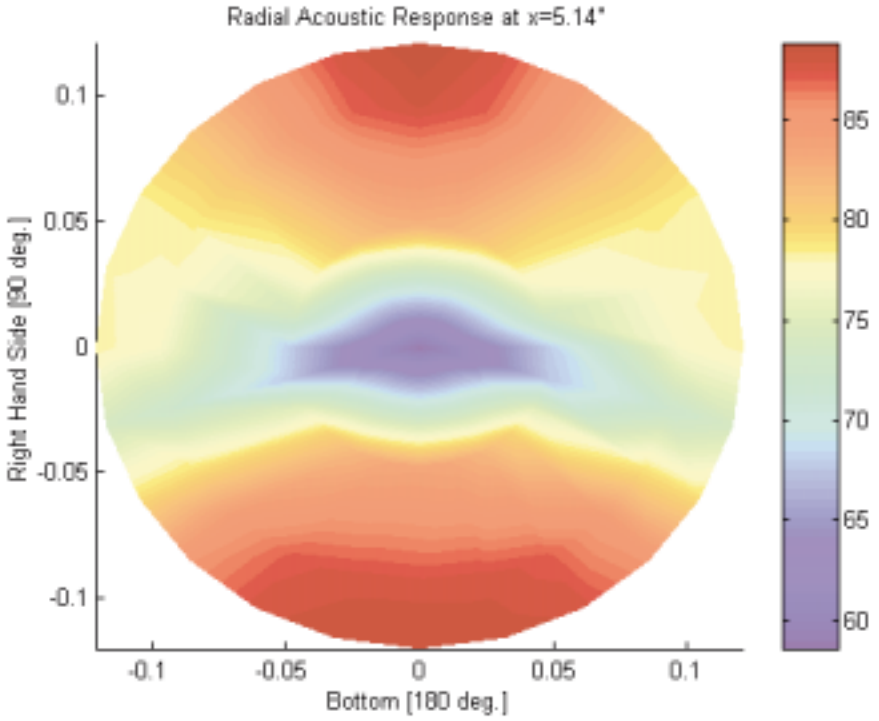

Figure 4.32 Radial internal acoustic simulation at 1/3 cylinder length (SPL in dB) at 1552 Hz.

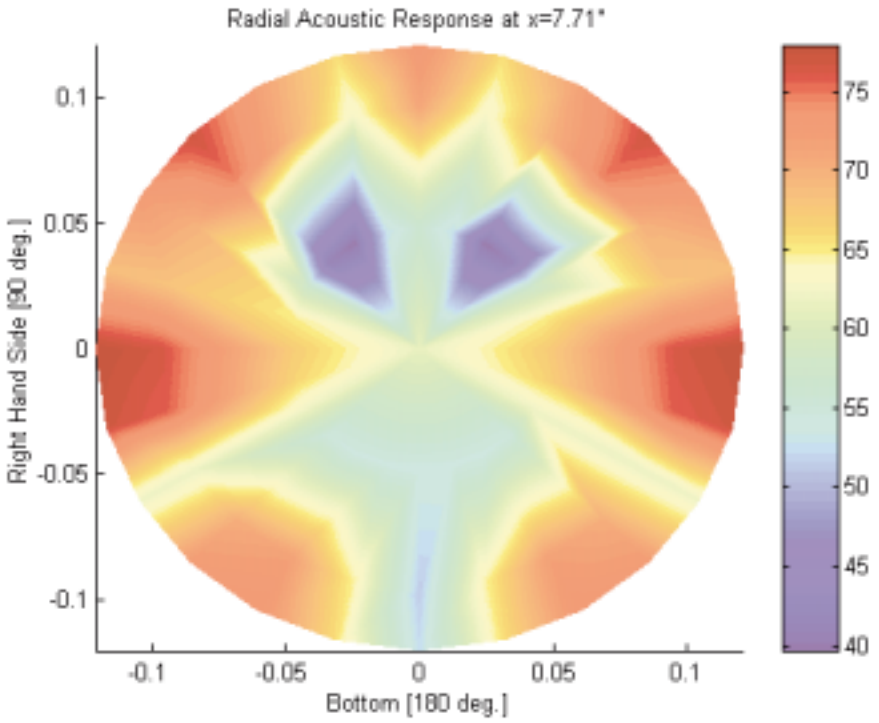

Figure 4.33 Radial internal acoustic simulation at 1/2 cylinder length (SPL in dB) at 1552 Hz.

4.10 Concluding Remarks on the Acoustic Model

In this chapter an experiment is performed to measure the acoustic response within a SS cylinder for a given structural excitation. The spatial structural accelerance of the cylinder is measured (using a roving accelerometer) and is used with the numerical model to predict the internal acoustic response of the SS cylinder. The predicted and experimental results are compared and an acoustic loss factor is determined for the aluminum cylinder interior space. It was found that the results predicted by the model and the experimental results are in close agreement. The model is able to predict the acoustic behavior within the cylinder for different positions and frequencies. Most of the resonances and anti-resonances are predicted with only slight shifts in frequency. This is indicative that the acoustic model is valid. In the following chapter, both the validated structural model (chapter 2) and acoustic model (chapter 3) are used to compute the acoustic response within a large scale cylinder which emulates a rocket payload fairing excited by PZT actuators.